EUMETSAT

OSI SAF

OCEAN AND SEA ICE

Geostationary Satellite Sea Surface Temperature Scientific Validation Report

Meteosat SST: OSI-206-a

GOES-East SST: OSI-207-a

Meteosat Indian Ocean SST: OSI-IO-SST

Version: 1.0
Date: 12/11/2018

S. Saux Picart, A. Marsouin

METEO FRANCE

Documentation change record

Version	Date	Authors	Description
0.1	9/7/2018	MF/CMS	Initial submitted version
1.0	12/11/2018	MF/CMS	Version after internal review (minor corrections)

Contents

List of Figures

List of Tables

1 Introduction

The EUMETSAT Satellite Application Facilities (SAFs) are dedicated centres of excellence for processing satellite data. They form an integral part of the distributed EUMETSAT Application Ground Segment. The Ocean and Sea Ice SAF, led by Météo-France/Centre de Météorologie Spatiale (MF/CMS), has the responsibility of developing, validating and distributing near real time products of Sea Surface Temperature (SST), radiative fluxes, wind and Sea Ice for a variety of platforms/sensors.

In this context OSI SAF is processing Sea Surface Temperature products from geostationary satellite from the EUMETSAT Meteosat Second Generation program and the US program of NASA and the National Oceanic and Atmospheric Administration (NOAA), Geostationary Operational Environment Satellite (GOES) in East position.

More specifically OSI SAF is providing the user community with the products presented in table 1

Table 1: Geostationary products summary.

Product ID	Satellite/instrument	Spatial coverage	Spatial sampling	Frequency	Reference
OSI-206-a	Meteosat-11 /SEVIRI	60°N to 60°S 60°W – 60°E	0.05° Lat-Lon	hourly	[AD.1]
OSI-207-a	GOES-16/ABI	60°N to 60°S 135°W – 15°W	0.05° Lat-Lon	hourly	[AD.1]
OSI-IO-SST	Meteosat-08 /SEVIRI	60°N to 60°S 19.5°W – 101.5°E	0.05° Lat-Lon	hourly	

1.1 Purpose and scope of the document

This document is the scientific validation report for the OSI SAF geostationary SST products.

Table 2: Threshold, target and optimal accuracies define respectively: the lower limit of usefulness, the main reference for assessment at EUMETSAT and the optimal performance reachable in theory provided the instrument characteristics. Extracted from [AD.1].

Product ID	Threshold accuracy. Monthly bias, SD	Target accuracy. Monthly bias, SD	Optimal accuracy. Monthly bias, SD
OSI-206-a OSI-207-a	1K, 1.5K	0.5K, 1.0K	0.1K, 0.5K
OSI-IO-SST	The above values are considered		

The intention of this report is to evaluate the quality of the OSI SAF geostationary products and their compliance with the product requirement of the third Continuous Development and Operation Phase (CDOP-3) which are summarised in table 2.

This document is complemented by the Algorithm Theoretical Basis Document for GOES-16 Sea Surface Temperature [RD.1] and the Geostationary Sea Surface Temperature Product User Manual [RD.2].

1.2 Reference documents

Ref	Title	Code
[RD.1]	Algorithm Theoretical Basis Document for GOES-16 Sea Surface Temperature	SAF/OSI/CDOP3/SCI/MA/328
[RD.2]	Geostationary Sea Surface Temperature Product User Manual	SAF/OSI/CDOP3/MF/TEC/MA/181

1.3 Applicable documents

Ref	Title	Code
[AD.1]	OSI SAF CDOP 3 Product Requirement Document, version 1.3	SAF/OSI/CDOP3/MF/MGT/PL/2-001
[AD.2]	OSI SAF Service Specification version 1.5	SAF/OSI/CDOP3/MF/MGT/PL/003

1.4 Acronyms

AVHRR	Advanced Very High Resolution Radiometer
BT	Brightness Temperature
CDOP	Continuous Development and Operation Phase
GOES	Geostationary Operational Environment Satellite
GTS	Global Telecommunication System
IR	Infra-Red
MF/CMS	Météo France/Centre de Météorologie Spatiale
MDS	Matchup DataSet
NOAA	National Oceanic and Atmospheric Administration
NWP	Numerical Weather Prediction
OSI SAF	Ocean and Sea Ice Satellite Application Facility
OSTIA	Operational Sea Surface Temperature and Sea Ice Analysis
QL	Quality Level
RTTOV	Radiative Transfer for TOVS
SAF	Satellite Application Facility
SDI	Saharan Dust Index
SEVIRI	Spinning Enhanced Visible and InfraRed Imager
SSES	Sensor Specific Error Statistics
SST	Sea Surface Temperature
SD	Standard Deviation
TIROS	Television Infrared Observation Satellite
TOVS	TIROS Operational Vertical Sounder

2 Overview of SST retrieval

In this section a brief overview of processing of SST for geostationary satellite and the creation of matchup dataset used in this report for validation. All the details are given in [RD.1].

2.1 Sea surface temperature computation

SST is computed for all clear-sky water pixels. Clear-sky pixels are identified using an external cloud mask as input to the processing. A cloud mask control procedure is used to assign a lower quality level to pixels which are dubious (thin cloud, dust aerosols,...). It consists of a series of tests that consider various quantities such as the local values of the gradient, temperature, probability of ice, etc. The quality level is provided at the pixel level with increasing reliability from 2 (="bad") to 5 (="excellent"); 0 means unprocessed and 1 means cloudy. Quality levels give the user a simple means of filtering the data. Users are advised to use quality levels 3 to 5 for quantitative applications. These quality levels are used in the analysis presented in the following sections, and only results of validation for quality levels 3 to 5 are shown.

For all geostationary sattelite, the computation of SST is based on a quasi-linear algorithm using brightness temperatures such as the ones presented in McCain et al. (1985); Walton et al. (1998). The generic form of the algorithm is:

$$\hat{\mathrm{x}} = a_0 + \mathbf{a}^\top \mathbf{y}_0 \tag{1}$$

where, $\hat{\mathrm{x}}$ is the estimated SST, a_0 is an offset coefficient, $\mathbf{a}$ is a column vector of weighting coefficients and $\mathbf{y}_0$ contains the observed BTs. The coefficients contained in the vector $\mathbf{a}$ are potentially functions of SST climatology and satellite zenith angle.

This type of algorithm, when used for global applications, induces regional and seasonal biases (e.g. Marsouin et al. (2015)). In order to correct for these, an algorithm correction method is used (Le Borgne et al., 2011). It relies on brightness temperature simulations from the RTTOV radiative transfer model using NWP atmospheric profiles and OSTIA SSTs (Donlon et al., 2012). Simulations are performed for each clear sky pixel identified as such with the cloud mask. Simulations are not perfect, due to model output errors, RTTOV errors and instrument calibration errors. They are therefore adjusted using an empirical approach based on averaging the simulated minus observed BT differences over 3 days centred on the day being processed. The correction is calculated as the difference between the retrieved SST from simulated adjusted BTs and the SST analysis used as input to the simulations.

2.2 Geostationary SST products

OSI SAF process data from three geostationary satellites: currently GOES-16 (in East position), Meteosat-8 on the Indian Ocean and Meteosat-11 over the Atlantic Ocean. The field of view of the three satellites are illustrated on Figure 1. Data are processed at full spatial resolution and aggregated as hourly product on a regular lat/lon grid.

Details about the products can be found in the Product User Manual [RD.2].

2.3 The match-up data set (MDS)

All validation procedures require a MDS has been elaborated. In an operational prospective, the MDS gathers in situ SST measurements from ship, moored buoys and drifting buoys available through the Global Telecommunication System (GTS). Collocated full resolution satellite information is added in a 3 hours time frame around the measurement. It consists in all the variables included in the intermediate workfile extracted in a box around the in situ measurements. The

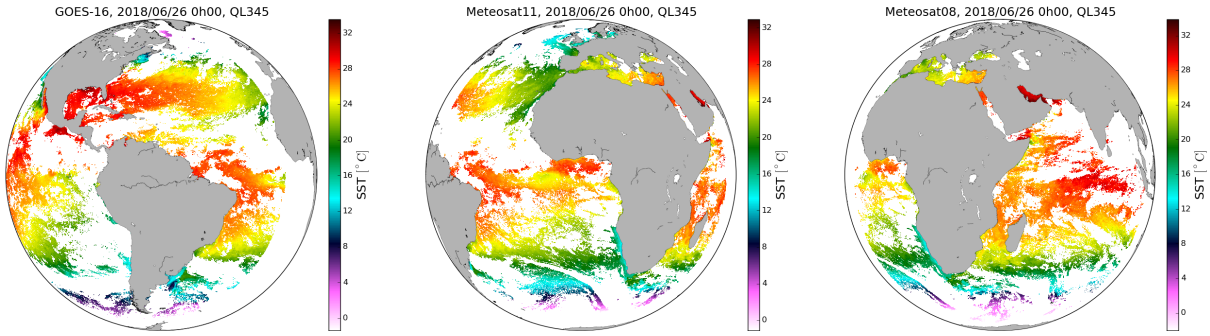

Figure 1: SST from GOES-16 (left), Meteosat-11 (left), and Meteosat-8 (right).

MDS for day d is currently elaborated with a five days delay ($d+5$) to ensure all in situ data are available through GTS. For the purpose of operational validation:

- Only drifting buoys are considered.
- Only the central SST of each box is used.
- Night-time and day-time algorithm are validated separately.

All subsequent results are based on the exploitation of the MDS.

3 Assessment of OSI SAF geostationary SST products

3.1 Statistics of comparison

The SST retrieved is assessed in terms of its difference to in situ measurements from drifting buoys. Normal statistics (bias and standard deviation (SD) of the difference (ΔSST = $SST_{sat} - SST_{in\,situ}$) are computed.

These statistics are usually computed on the whole disk of view for various time intervals (month, trimester or whole duration) and presented hereafter.

Only satellite SST quality level 3 to 5 are assessed unless otherwise stated. SSES biases have not been applied.

3.2 Overall statistics

In this section we present the results for the entire field of view of each satellite and a time period as follow:

- GOES-16 (OSI-207-a): from 2018/1/11 to 2018/6/10
- Meteosat-11 (OSI-206-a): from 2018/2/1 to 2018/6/10
- Meteosat-8 (OSI-IO-SST): from 2017/3/1 to 2018/6/10

Table 3 shows the result of comparison to drifting buoy measurements for pixel quality level 3, 4 and 5 together. For Meteosat-8 and 11 products the bias and standard deviation are of the same order of magnitude: bias 0.1K and SD 0.53K with a slightly higher SD during day-time. Statistics are better for GOES-16 product with a bias $<$ 0.1K and a SD of the order of 0.45K. The reason explaining these better results is the use of a three channel algorithm (see [RD.1]).

Table 3: Statistics of the difference between satellite SST and drifting buoy measurements computed: Mean (Bias), standard deviation (SD). N is the number of matchups.

	Night			Day		
	N	Bias	SD	N	Bias	SD
GOES-16 (OSI-207-a)	87463	-0.03	0.46	130686	0.07	0.45
Meteosat-11 (OSI-206-a)	82535	-0.10	0.53	120072	-0.09	0.56
Meteosat-8 (OSI-IO-SST)	213259	-0.11	0.52	281152	-0.12	0.58

Tables 4, 5 and 6 contain the same statistics as table 3 split by quality level. One can notice the clear improvement of the statistics as the quality level goes up. Readers' attention is drawn to the degraded statistics for quality level pixels equal to 2 (bias around -0.4K and SD around 0.85K), which should be used use with precaution.

Table 4: GOES-16. Statistics of the difference between satellite SST and drifting buoy measurements presented per quality level (QL). Mean (Bias), standard deviation (SD). N is the number of matchups.

	Night			Day		
QL	N	Bias	SD	N	Bias	SD
5	35975	-0.04	0.41	55515	0.04	0.40
4	29566	-0.02	0.45	43862	0.08	0.44
3	21922	-0.02	0.55	31309	0.10	0.55

Table 5: Meteosat-11. Statistics of the difference between satellite SST and drifting buoy measurements presented per quality level (QL). Mean (Bias), standard deviation (SD). N is the number of matchups.

	Night			Day		
QL	N	Bias	SD	N	Bias	SD
5	38282	-0.08	0.44	58520	-0.06	0.51
4	24983	-0.09	0.54	35336	-0.12	0.55
3	19270	-0.13	0.66	26216	-0.13	0.67

Table 6: Meteosat-8. Statistics of the difference between satellite SST and drifting buoy measurements presented per quality level (QL). Mean (Bias), standard deviation (SD). N is the number of matchups.

	Night			Day		
QL	N	Bias	SD	N	Bias	SD
5	105490	-0.06	0.42	132087	-0.04	0.46
4	62270	-0.13	0.55	89417	-0.18	0.61
3	45499	-0.17	0.67	59648	-0.21	0.74

Time series of 10-days statistics are presented on Figure 2, 3 and 4 for quality level 3, 4 and 5 together and for day and night time separately. For GOES-16 (figure 2) the bias and SD are stable over the period considered during night-time. A small variation of the bias is observed during day-time.

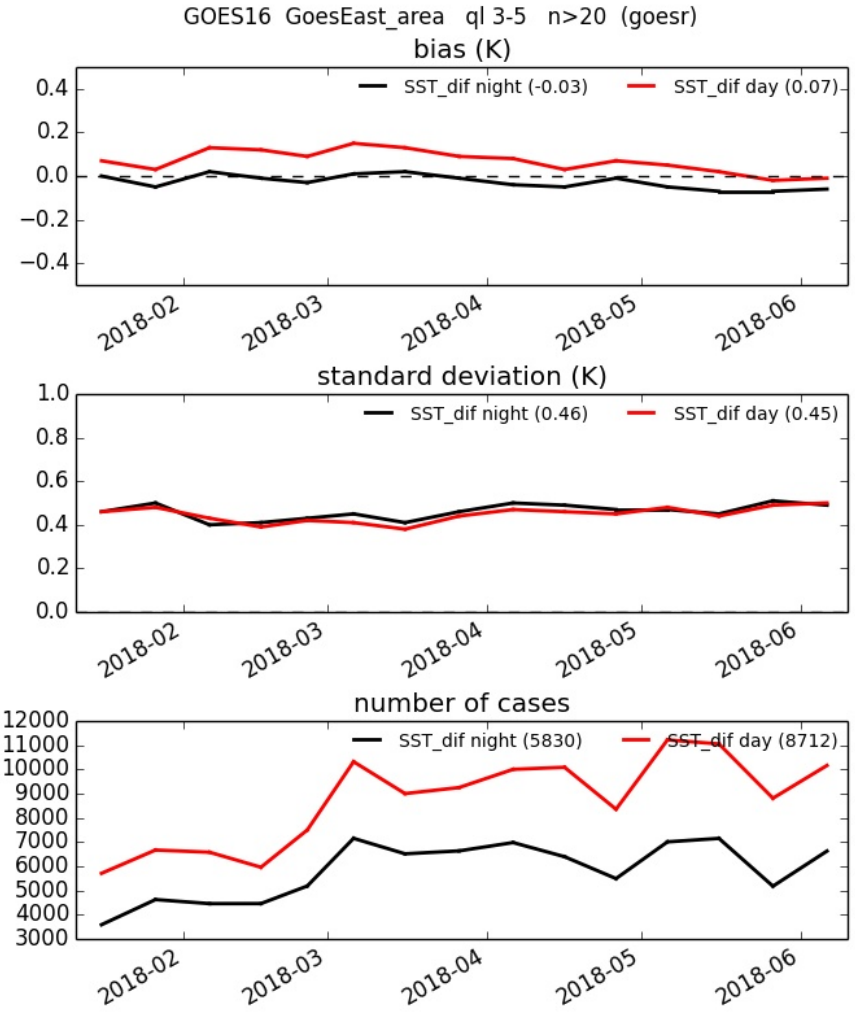

Figure 2: GOES-16. Time evolution of the mean bias (top), SD (middle) and number of matchups (bottom) for the comparison to drifting buoy measurements.

For Meteosat products the statistics are also quite stable. Some negative biases, more visible during day-time, are observed during the last decade of May (corresponding to an increase in SD). This is possibly due to some outbursts of atmospheric Saharan dusts in the Mediteranean Sea illustrated by the Saharan Dust Index (Merchant et al., 2006, SDI,) presented on figure 5 for two dates in May 2018. On this figure one can see high values of SDI situated in the Eastern part of the Mediterranean Sea on the 23rd of May. On the 29th of May a new outburst occurs in the Western part of the Mediterranean Sea, off the coast of Tunisia.

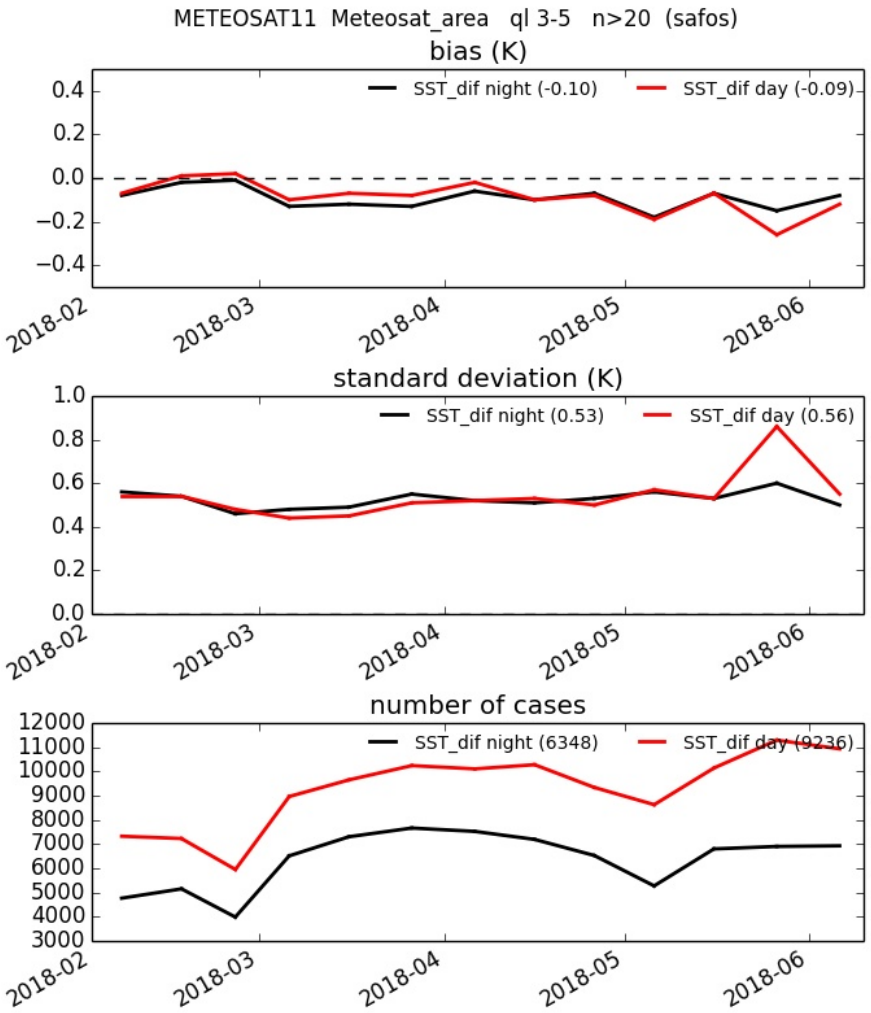

Figure 3: Meteosat-11. Time evolution of the mean bias (top), SD (middle) and number of matchups (bottom) for the comparison to drifting buoy measurements.

Saharan Dusts cause an extra absorption of the IR radiation leading to an underestimation of the retrieved SST. However Sharan dusts alone may not explain fully the magnitude of the observed bias during day-time and the fact that it is less visible during night-time.

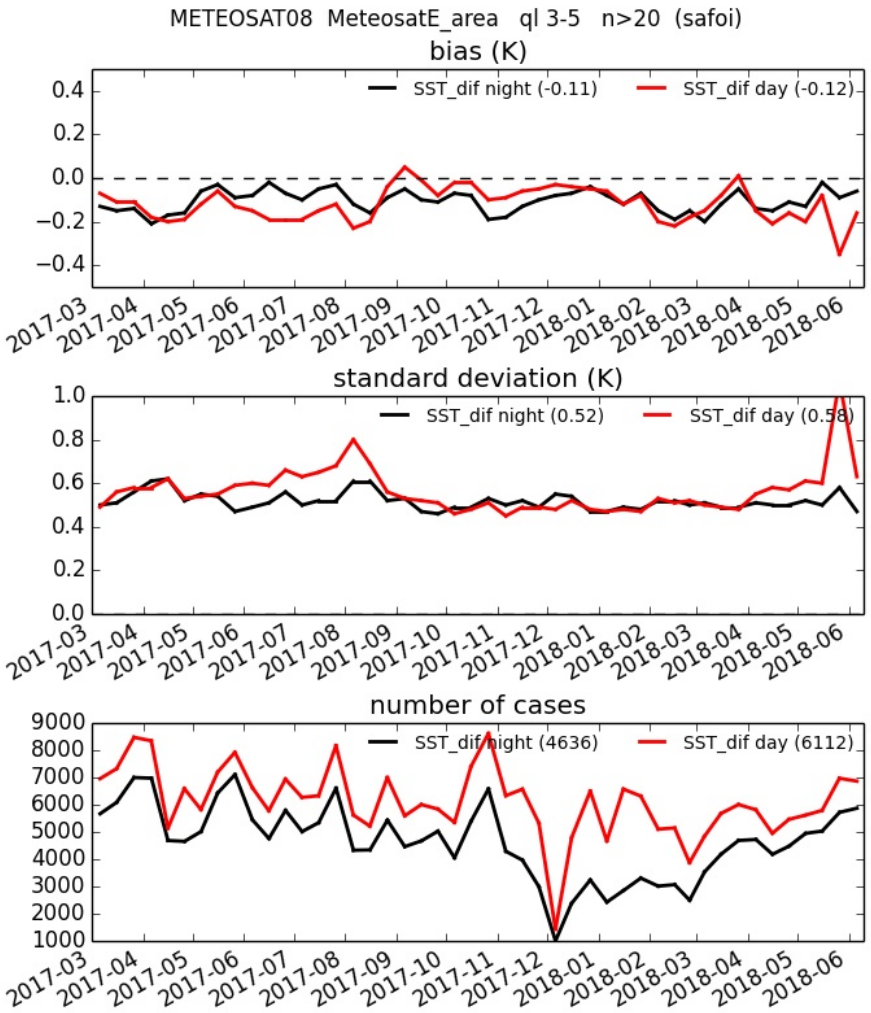

Figure 4: Meteosat-8. Time evolution of the mean bias (top), SD (middle) and number of matchups (bottom) for the comparison to drifting buoy measurements.

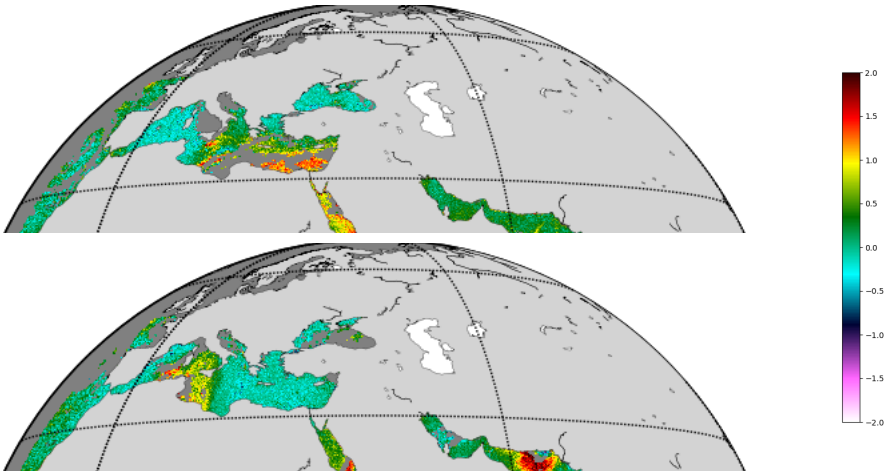

Figure 5: Saharan Dust Index from Meteosat-8 for 23/5/2018 (top) and 29/5/2018 (bottom).

3.3 Regional statistics

In this section results of the comparisons to drifting buoys are presented regionally. Monthly maps of the bias with respect to drifting buoys measurements are presented on Figure 6. The bias stay small across the domains with values very occasionally reaching 1K. It is to be noted that large biases are quite consistently associated with a low number of collocations (see figure 8) and a high standard deviation (see figure 7). In particular one can notice the very low number of data points in the Southern Seas also corresponding to high satellite zenith angle.

One can notice a negative bias in the Northern hemisphere and a positive bias in the Southern hemisphere. Further investigations (not shown here) have shown the seasonality of this observation: it is more pronounced during late spring and summer months. While these biases are not large, they remain unexplained. Similar feature is also apparent on Metop/AVHRR validation results.

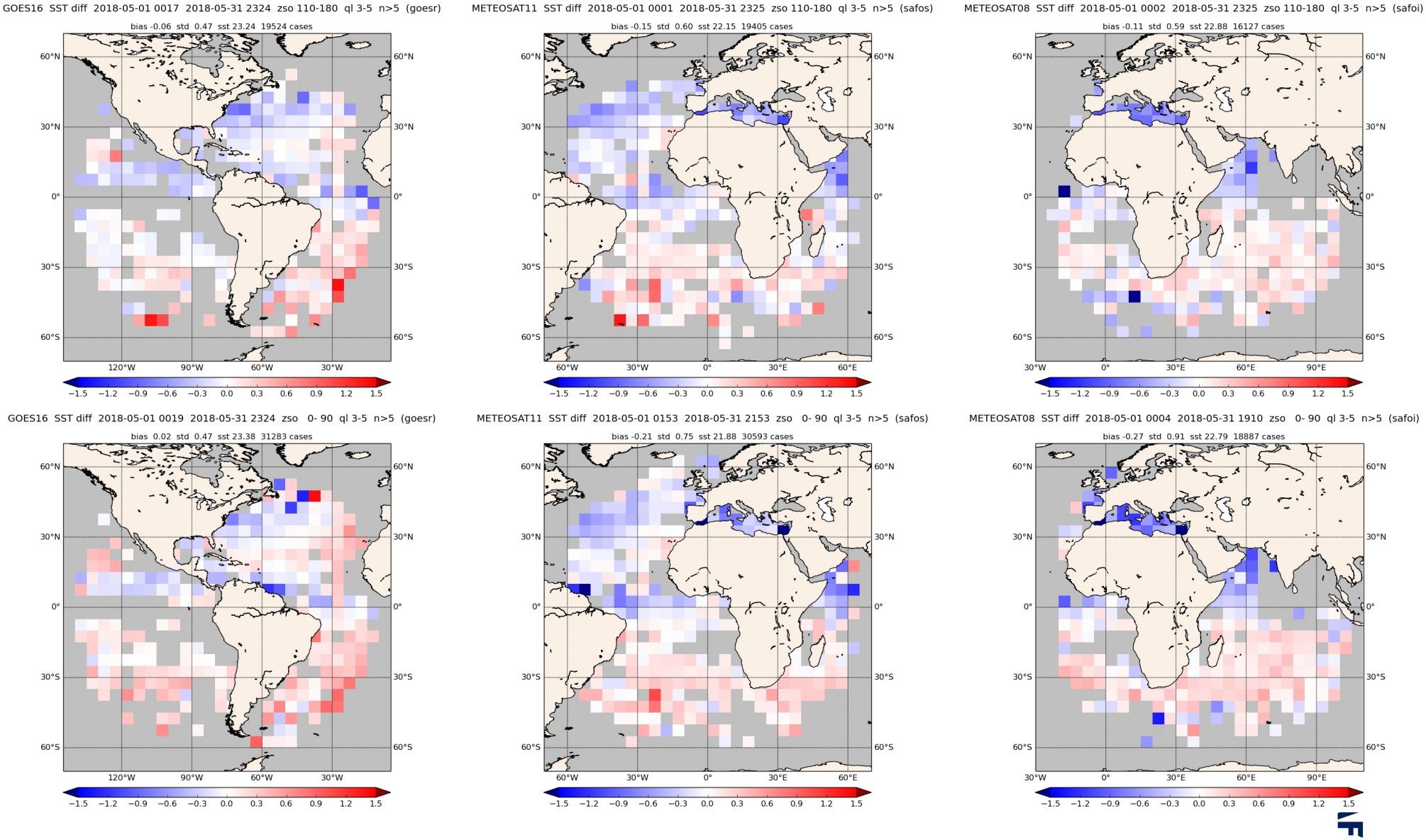

Figure 6: Monthly bias: satellite SST minus drifting buoys SST for night-time (top) and day-time (bottom): GOES16 (left), Meteosat 11 (left), and Meteosat 8 (right).

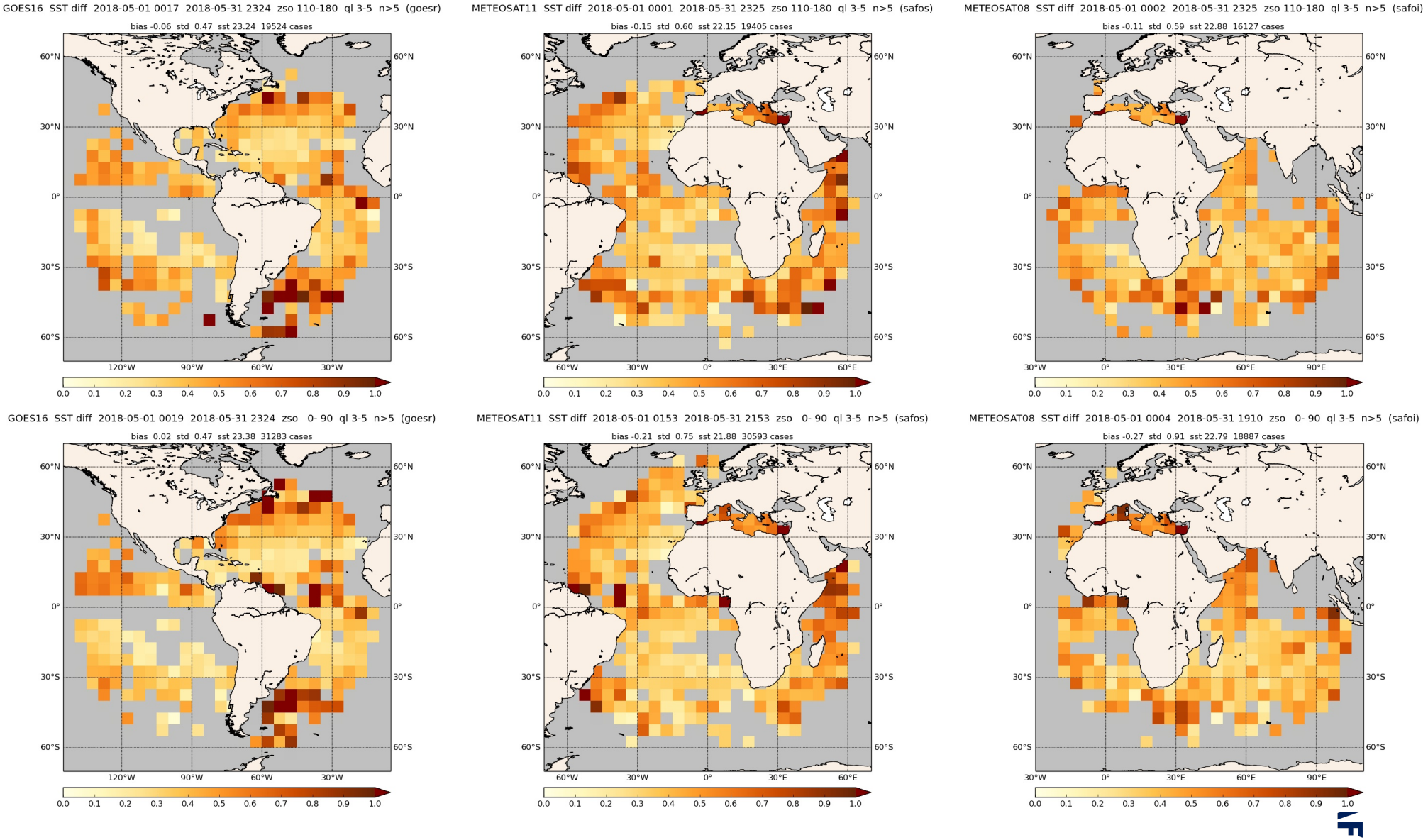

Figure 7: Monthly standard deviation: satellite SST minus drifting buoys SST for night-time (top) and day-time (bottom): GOES16 (left), Meteosat 11 (left), and Meteosat 8 (right).

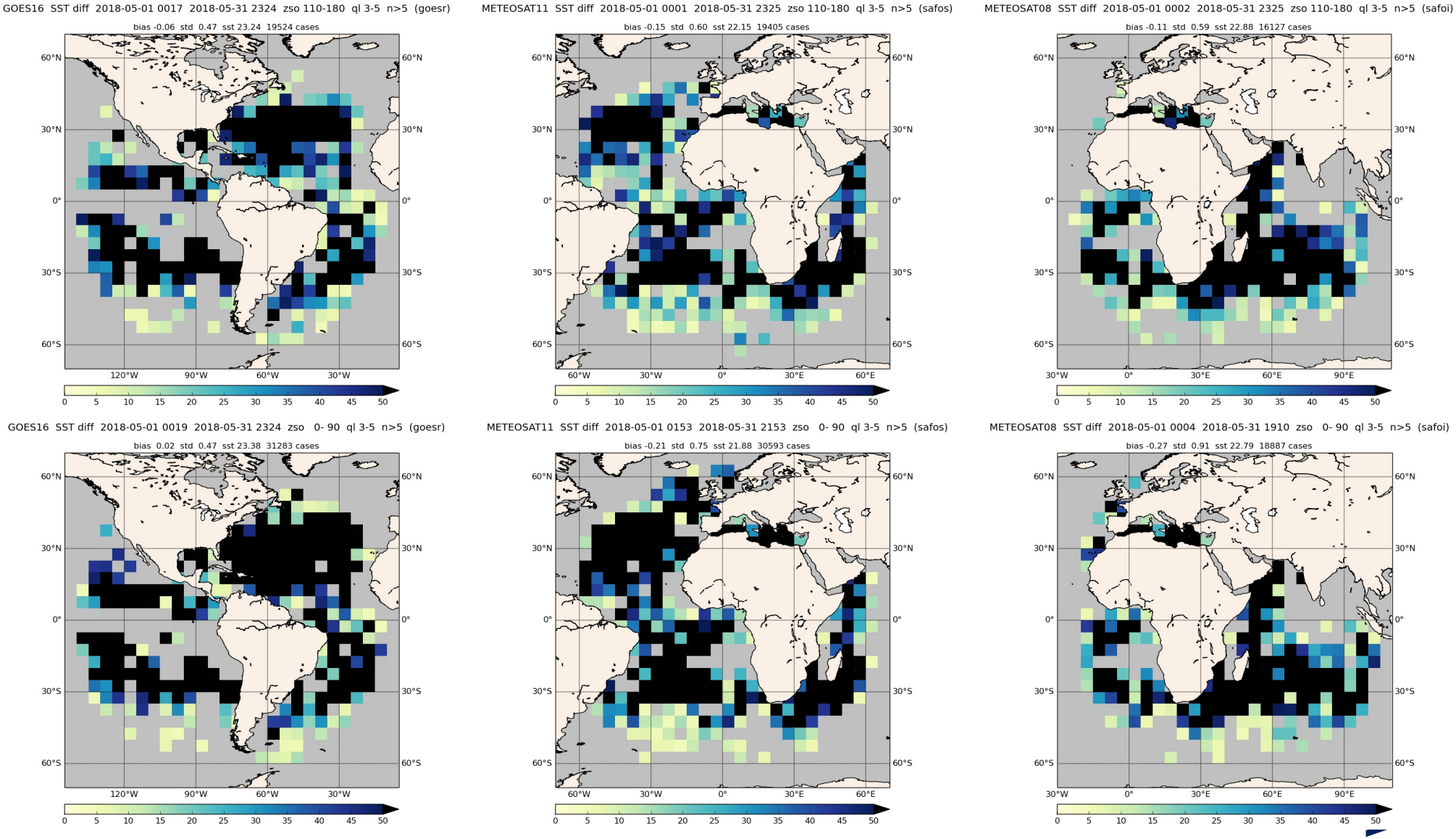

Figure 8: Monthly number of matchups: satellite SST minus drifting buoys SST for night-time (top) and day-time (bottom): (left), Meteosat 11 (left), and Meteosat 8 (right).

3.4 SST dependencies

Another informative way of looking at the comparison with in situ data is to plot the difference satellite SST minus in situ SST as a function of some other variables. Figures 9, 10 and 11 display such plots with respect to in situ SST, satellite zenith angle, latitude and longitude for GOES-16, Meteosat-11 and Meteosat-8 respectively.

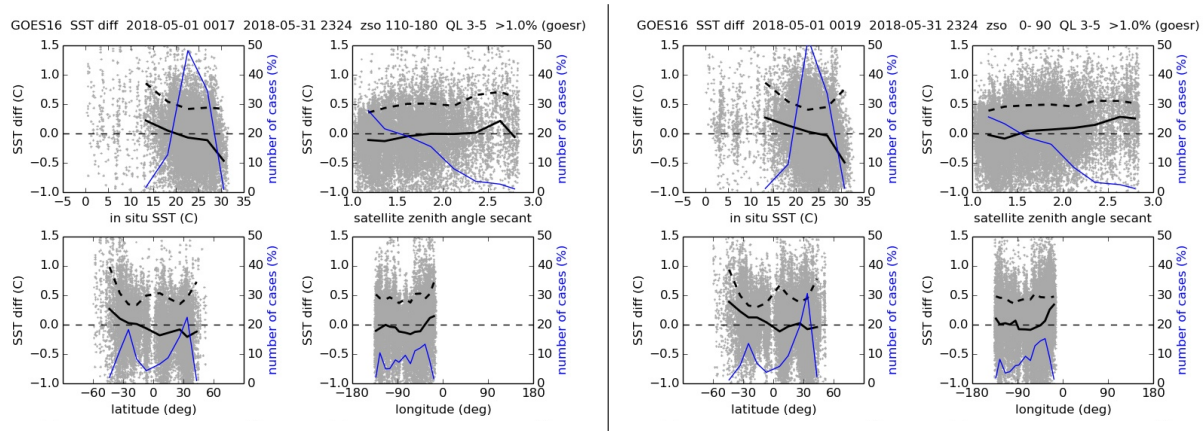

Figure 9: May 2018. Bias (black line) and standard deviation (black dashed line) of the difference GOES-16 SST minus drifting buoy SST plotted as a function of in situ SST, satellite zenith angle, longitude and latitude: night -time on the left and day-time on the right.

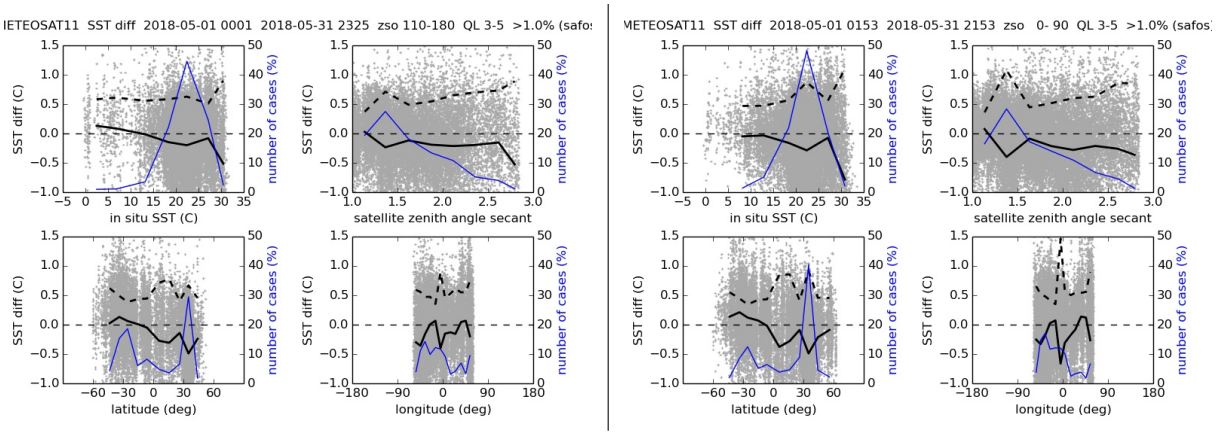

Figure 10: May 2018. Bias (black line) and standard deviation (black dashed line) of the difference Meteosat-11 SST minus drifting buoy SST plotted as a function of in situ SST, satellite zenith angle, longitude and latitude: night -time on the left and day-time on the right.

For GOES-16 product: dependencies are small with respect to latitude and longitude. The only noticeable dependencies are for in situ SST at the extremes (where few collocation data is available) and for satellite zenith angle during day-time.

For Meteosat products: the longitude and latitude dependencies are very different between satellites due to their respective field of view and the position of the continents in them. On Meteosat-11 plots, one can notice a drop of the bias around 35 degree of latitude and around 0 degree of longitude (mostly during day-time). This is the signature of the Mediterranean Sea which, as seen in section 3.3, is a region with a negative bias more pronounced during day-time. This is also visible on Meteosat-8 satellite zenith angle plots (Figure 11) where a drop in the bias during the day is observed for a secant of about 2 (corresponding to a satellite zenith angle

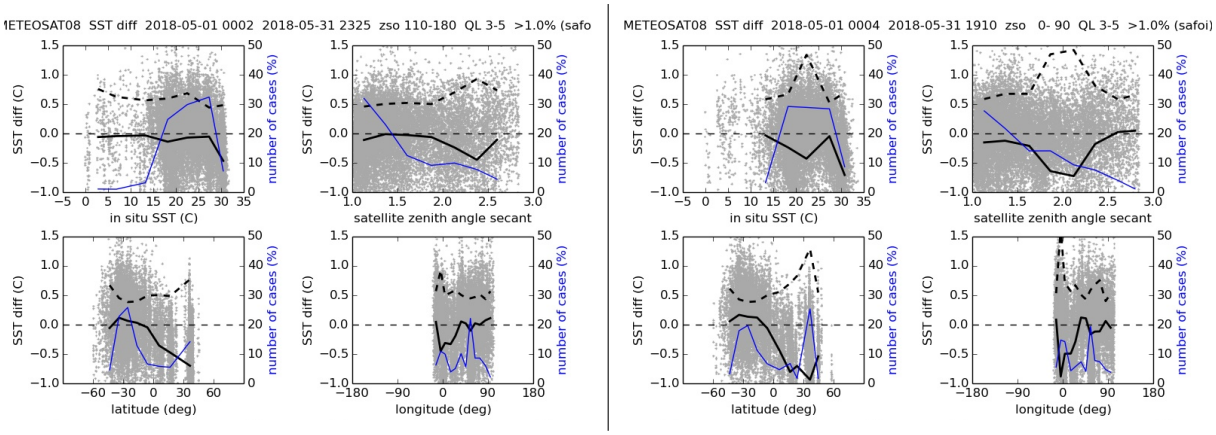

Figure 11: May 2018. Bias (black line) and standard deviation (black dashed line) of the difference Meteosat-8 SST minus drifting buoy SST plotted as a function of in situ SST, satellite zenith angle, longitude and latitude: night -time on the left and day-time on the right.

of 60 degrees). Despite the above mentioned minor features, these plots do not show any strong anomalies.

4 Conclusion

The quality assessment of OSI SAF geostationary SST products (GOES-16, Meteosat-8 and Meteosat-11) shows coherent and stable results over time within the OSI SAF CDOP-3 requirements.

For Meteosat products, the comparison to drifting buoys is consistent with the state of the art and in particular with Merchant et al. (2009); Le Borgne et al. (2011).

GOES-16 product are noticeably better (in term of standard deviation) than Meteosat products. GOES-16 carries a new generation instrument, the Advanced Baseline Imager (ABI), which has more channel suitable for SST retrieval than Meteosat/Spinning Enhanced Visible and Infra Red Imager (SEVIRI). The algorithm designed for GOES-16/ABI make use of three channels (8.5, 10.3 and 12.3μm) making it more robust to varying atmospheric conditions (water vapour in particular).

References

Donlon, C. J., Martin, M., Stark, J., Roberts-Jones, J., Fiedler, E., and Wimmer, W. (2012). The operational sea surface temperature and sea ice analysis (OSTIA) system. *Remote Sensing of Environment*, 116:140—-158.

Le Borgne, P., Roquet, H., and Merchant, C. (2011). Estimation of sea surface temperature from the spinning enhanced visible and infrared imager, improved using numerical weather prediction. *Remote Sensing of Environment*, 115(1):55–65.

Marsouin, A., Le Borgne, P., Legendre, G., Péré, S., and Roquet, H. (2015). Six years of OSI-SAF METOP-A AVHRR sea surface temperature. *Remote Sensing of Environment*, 159:288–306.

McCain, E. P., Pichel, W. G., and Walton, C. C. (1985). Comparative performance of AVHRR-based multichannel sea surface temperature. *Journal of Geophysical Research*, 90:11587–11601.

Merchant, C. J., Embury, O., Le Borgne, P., and Bellec, B. (2006). Saharan dust in nighttime thermal imagery: Detection and reduction of related biases in retrieved sea surface temperature. *Remote Sensing of Environment*, 104(1):15–30.

Merchant, C. J., Le Borgne, P., Roquet, H., and Marsouin, A. (2009). Sea surface temperature from a geostationary satellite by optimal estimation. *Remote Sensing of Environment*, 113(2):445–457.

Walton, C. C., Pichel, W. G., Sapper, J. F., and May, D. A. (1998). The development and operational application of nonlinear algorithms for the measurement of sea surface temperatures with the NOAA polar-orbiting environmental satellites. *Journal of Geophysical Research*, 103:27999–28012.